

Damping of surface waves by floating particlesBruce R. Sutherland^{1,2,*} and Neil J. Balmforth^{3,4}¹*Department of Physics, University of Alberta, Edmonton, Alberta, Canada T6G 2E1*²*Department of Earth & Atmospheric Sciences, University of Alberta, Edmonton, Alberta, Canada T6G 2E3*³*Department of Mathematics, University of British Columbia, Vancouver, British Columbia, Canada V6T 1Z2*⁴*Department of Earth, Ocean, and Atmospheric Sciences, University of British Columbia, Vancouver, British Columbia, Canada V6T 1Z4*

(Received 26 August 2018; published 15 January 2019)

Laboratory experiments are performed examining the enhanced damping of surface waves by floating spherical particles. Without particles, wave amplitudes decay exponentially in time; with the particles, the dissipation is enhanced such that waves are arrested in finite time. Initially the decay is exponential with an e-folding time that is inversely proportional to the depth of the particle layer, but independent of particle size. At later times and lower amplitudes, the decay turns into a power law $(t_s - t)^q$, with exponent lying between $q \simeq 2$ and 3. The stopping time t_s also decreases with increasing particle layer depth.

DOI: [10.1103/PhysRevFluids.4.014804](https://doi.org/10.1103/PhysRevFluids.4.014804)**I. INTRODUCTION**

As the extent of Arctic sea ice decreases, more of the sea surface is exposed to winds that, over a larger fetch, can generate more energetic waves. These waves, when incident upon sea ice can, in turn, act to fracture, erode, and break apart solid ice and ice floes in the marginal ice zone, thus enhancing further melting [1–4]. For this reason there have been several recent observational, experimental, and theoretical studies aimed at understanding the propagation and attenuation of waves in the marginal ice zone [5–9]. Given the complexity of the dynamics governing the attenuation of the waves, it is often assumed that the amplitude of waves incident upon an ice floe decays exponentially in space [6,10], or, equivalently, decays exponentially in time in a frame of reference moving with the group velocity of the waves. This is consistent with theoretical models that represent the ice floe layer as a viscous fluid [11] or as a viscoelastic sheet [12–14]. Such models might be suitable to model the damping of waves with amplitude larger than the depth of the ice layer, although its universal applicability has recently been questioned [15]. Furthermore, the common observation of the sudden arrest of waves in a glass of water and ice suggests that new dynamics dominate the attenuation of waves covered with blocks of ice when their amplitude is comparable to the depth of the ice layer. The study presented here examines these dynamics through a simple scaling theory complemented by laboratory experiments.

The damping of waves by ice has previously been examined through experiments in which the laboratory was cooled below freezing to create a surface ice layer in a long tank with a wave maker at one end and a dissipating beach at the other [16–19]. Analysis of the attenuation of the progressive waves assumed an exponential decay at the outset. However, the attenuation rate predicted by the viscous theory [11] was found to be much smaller than observed for low frequency waves [18]. The interpretation of the experiments was further complicated by the tendency of the waves to pile up

*bruce.sutherland@ualberta.ca

the ice toward the far end of the tank leading to ice cover of nonuniform depth along the length of the tank.

Assuming that the thermodynamics of ice melting and freezing plays an insignificant role in the wave mechanics, floating particles provide an alternative material with which to conduct laboratory experiments. Furthermore, the temporal decay of standing waves can be observed at high spatial and temporal resolution with a stationary camera and, unlike progressive waves, standing waves do not drive a net horizontal transport of particles. In the current paper, we therefore study the effect of multiple layers of floating particles on the sloshing dynamics of water in a rectangular tank.

The influence of a layer of bubbles (i.e., a foam) on the damping of standing waves has recently been examined by Sauret *et al.* [20] and Viola *et al.* [21]. In these studies, it was concluded that viscous damping in the plateau borders moving against the walls of the container were primarily responsible for damping sloshing motions, with the damping rate dependent on the depth of the layer of bubbles. Recent studies also noted that wave motion can be arrested in a finite time due to capillary effects at the side walls with or without foam [21–23]. Although the dynamics of damping by foam is expected to be very different from damping by loose floating particles, we likewise observe a layer-depth-dependent effect of the particles on damping rates, and a rapid arrest of waves when their amplitude becomes small compared to the depth of the particle layer. Here we posit that the finite-time arrest is primarily due to processes within the bulk of the particles and not due to those near the side walls of the tank.

In Sec. II we develop a general theory for the time evolution of the wave amplitude as it is influenced by linear and nonlinear damping. The experiment setup and analysis methods are described in Sec. III along with results characterizing the attenuation of the waves as it depends upon particle depth. Various scalings are then discussed in Sec. IV, whereupon it is shown that the finite-time arrest is most likely due to the flow of interstitial fluid being forced between periodically consolidating and separating particles. The main results are summarized in Sec. V with a tentative application of this work to predicting damping by surface waves in the marginal ice zone.

II. PHYSICAL SETTING

In the absence of foam or floating particles and ignoring capillary effects, waves in a tank lose their energy due to viscous forces acting within the bulk of the fluid and on the sides and bottom of the tank. For a mode sloshing in a tank that is sufficiently deep compared to the wavelength of the disturbance that motion along the bottom is negligibly small, the main source of damping arises from the (Stokes) viscous boundary layers against the side of the tank. If the tank has length L in the direction of the seiche and width W in the perpendicular direction, and the slosh has wave number $k = \pi/L$ and frequency ω , the e-folding damping time is of the order [20]

$$\tau_0 \sim \frac{LW}{2(L+W)\sqrt{\nu\omega}}, \quad (1)$$

in which $\omega = \sqrt{gk}$ for deep water waves and ν is the kinematic viscosity.

If floating particles are present in the fluid, additional losses occur. Some models for wave attenuation in the marginal ice zone treat the particle layer as a flexible surface film providing a no-slip upper boundary condition [24,25]. In this case the (linear) damping time scale is of the order

$$\tau_k \sim \frac{1}{k\sqrt{\nu\omega}}, \quad (2)$$

which for laboratory experiments of a surface seiche would be proportional to τ_0 if the spanwise extent of the tank was very large. On a more microscopic level, losses also occur due to the motion of the particles near the tank side walls and of fluid percolating between the particles as they alternately consolidate and separate due to the changing surface area of the wave. Some of these processes are illustrated schematically in Fig. 1. Particles near the side walls induce a shear flow in the small gap between the particles and the rigid wall. This, together with the pressing of the

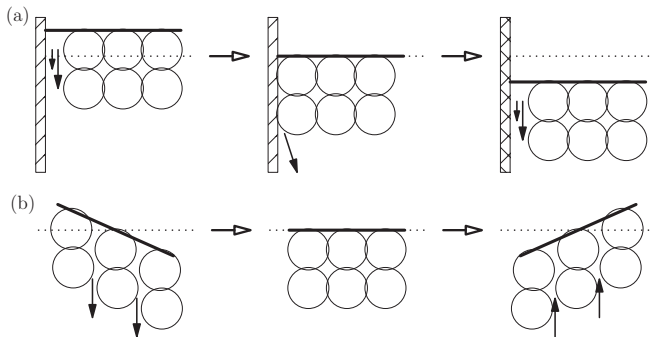


FIG. 1. Conceptual schematics showing possible mechanisms for wave energy dissipation by floating particles. (a) Descending surface near tank wall to the left showing induced shear flow between particles and the side wall and contact of particles with wall when surface is at equilibrium depth. (b) Flow alternately being extruded (downward arrows on left) and drawn in (upward arrows on right) between particles as the wave flattens (left to middle panel) and steepens (middle to right panel). In each schematic, the horizontal dotted line denotes the surface in the absence of waves and the thick solid line denotes the surface with waves present.

particles against the side wall as the pack consolidates, introduce dissipative effects around the perimeter [Fig. 1(a)]. Similar effects occur within the bulk of the floating particle layer as sheets of particles are periodically pulled apart and pressed together by the straining and shearing action of the sloshing mode [Fig. 1(b)].

The phenomenology in Fig. 1 suggests that relatively large amplitude waves may break apart the lattice of particles to furnish an enhanced but linear effective damping. However, at lower amplitudes, the particles can lock back up into jammed states, with the fluid flow between particles providing a nonlinear source of damping. The latter then forces motion to stop in finite time in the final stages of sloshing.

For a framework within which to discuss the experimental results outlined presently, we consider the energy equation for a sloshing mode. If the surface is displaced sinusoidally with a small amplitude $A(t) \equiv \mathcal{A} \sin \omega t$, the mean energy of a deep water wave is

$$\langle E \rangle \sim \rho (\mathcal{A} \omega)^2 L W / (2k). \quad (3)$$

We then adopt the equation for the amplitude evolution,

$$\frac{d\langle E \rangle}{dt} = -\langle \epsilon_2 \rangle - \langle \epsilon_p \rangle, \quad (4)$$

where ϵ_2 denotes the combined dissipation rate of all damping processes proportional to the squared mode amplitude (i.e., those that provide traditional linear damping terms), and ϵ_p represents any other (nonlinear) source of damping proportional to a different power $p < 2$ of \mathcal{A} . Thus

$$\frac{d}{dt} \tilde{\mathcal{A}}^2 = -\frac{2}{\tau_2} \tilde{\mathcal{A}}^2 - \frac{1}{\tau_p} \tilde{\mathcal{A}}^p, \quad (5)$$

in which $\tilde{\mathcal{A}} = \mathcal{A}/A_0$, with A_0 being the initial wave amplitude and τ_2 and τ_p are the effective damping times of the two types of processes. We refer to τ_2 as the “linear” damping timescale in the sense that if we neglect the last term in Eq. (5) then this becomes a linear equation of the function $\tilde{\mathcal{A}}^2$. For example, without particles, we omit the second term ($\tau_p \rightarrow \infty$) and prescribe τ_2 by (1), in which case τ_2 can be interpreted as an e-folding timescale.

The solution of (5) is

$$\mathcal{A} = A_0 \left[(1 + C) \exp\left(-\frac{t}{q\tau_2}\right) - C \right]^q, \quad (6)$$

in which $C = q\tau_2/\tau_p$ and $q = 1/(2 - p)$, which is positive under the assumption that $p < 2$. At early times ($t \ll q\tau_2$) the amplitude decreases in time according to $\mathcal{A} \simeq A_0(1 - t/\tau) \simeq A_0e^{-t/\tau}$, in which

$$\tau = \tau_2/(1 + C) \simeq \begin{cases} \tau_2, & C \ll 1, \\ \tau_p/q, & C \gg 1. \end{cases} \quad (7)$$

Equation (6) predicts the amplitude falls to zero in a finite time

$$t_s = q\tau_2 \ln(1 + 1/C) \simeq \begin{cases} q\tau_2 \ln(1/C), & C \ll 1, \\ \tau_p, & C \gg 1, \end{cases} \quad (8)$$

and the approach to zero behaves as a power law according to $\mathcal{A} \simeq A_0[(t_s - t)/\tau_p]^q$, which is valid if $(t_s - t) \ll q\tau_2$.

In the experiments presented below, we typically find that the stopping time is much larger than the e-folding time for initial exponential damping (i.e., $t_s \gg \tau$). This suggests that the experiments lie in the regime with $C \gg 1$ so that both τ and t_s are set by τ_p and not the linear damping timescale τ_2 , which is important only insofar as it demarks the separation between early-time exponential damping and the late-time power law approach to finite-time arrest. That said, although we find the amplitude decay follows a power law close to the stopping time, the reasons for the observed power law exponent remain elusive. Some attempt to provide physical insight follows in Sec. IV.

III. LABORATORY EXPERIMENTS

Most experiments were performed examining the decay in amplitude of a sloshing surface wave whose damping was enhanced by the presence of floating spherical hydrogel (hydrated sodium polyacrylate) beads from JellyBeadz®. Though not the focus of the analyses presented here, some experiments were also performed examining the enhanced damping of waves by the fine foam in a head of Guinness beer and by artificial snow (from SnoWonder®), which in its dry state is effectively finely ground sodium polyacrylate particles. Below we discuss the setup and analysis of experiments with hydrogel beads alone.

A. Experiment setup

Experiments were performed in an acrylic rectangular tank with interior dimensions measuring 23.75 by 18.05 cm in the horizontal and with height $H_T = 29.9$ cm. The tank was filled to a depth H with a mixture of salt water, red food coloring, as well as a small amount of dish soap added so as to reduce the effects of surface tension. Typically the depth was $H \simeq 23$ cm and the density was $\rho_0 \simeq 1.08$ g/cm³.

Floating spherical particles were then added. These were hydrogel beads initially hydrated with fresh water and, for some, blue food coloring. The resulting density of the particles was $\rho_p \simeq 1.0$ g/cm³, close to that of fresh water and their diameter was $d_p \simeq 1.6$ cm. Being composed mostly of water, the index of refraction of the particles was close to that of the ambient fluid and so it was possible to look through the particles in the tank seeing only those that were dyed blue. This enabled visualization of relative displacements of the dyed particles far from the side walls within the tank during the course of an experiment. The number of particles added was set so that they would lie approximately in an integer number of layers with each layer forming a hexagonal lattice. For an experiment with N_ℓ layers of particles, the depth was estimated to be $D = d_p[1 + (N_\ell - 1)\sqrt{2/3}]$, assuming an hexagonal close-packed configuration.

As a result of contact with salt water, the hydrogel beads absorbed some salt and consequently rejected some fresh water. However, this process was slow, taking on the order of an hour for a discernible change in the radii of the particles. Because the duration of any one experiment was, at most, on the order of 100 s, the particle size was assumed to be constant during an experiment. However, by recovering the particles and storing them overnight, their size decreased significantly

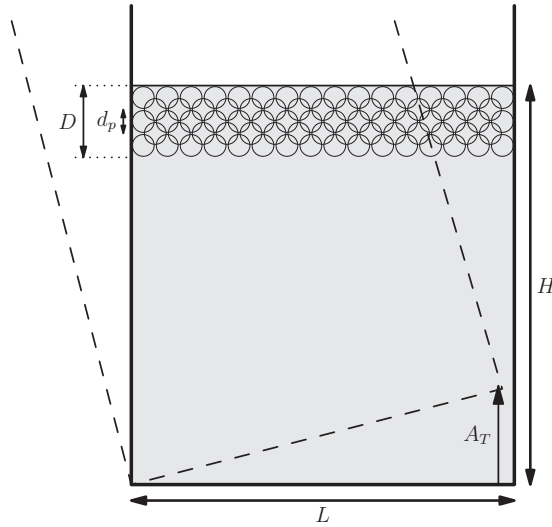


FIG. 2. Sketch of the experimental setup showing the level tank with five layers of beads spanning a depth D and the tilted tank (dashed lines) raised a distance A_T .

while still having a density much less than that of the ambient salt water. Thus in a separate series of experiments it was possible to reuse the particles having diameters of $d_p = 1.1$ cm and, with longer exposure to salt water, $d_p = 0.8$ cm.

After particles were added, some ambient fluid was removed so as to keep the height H of the surface approximately fixed. The tank was then tilted, pivoting either along the length or width of the tank. A support of height A_T was placed on the far side of the pivot, as illustrated in Fig. 2. Different supports were used with $A_T = 3.8, 5.7,$ and 8.9 cm. The system was then kept still until no motion was discernible within the tank.

At the start of an experiment the support was removed and the tank was rapidly returned to its untilted position. This set up a spanwise-uniform seiche in a rectangular domain of length L . The initial amplitude of the seiche was related to the support height A_T , but also depended upon the rate at which the tank was lowered to its upright position. Although a superposition of wave modes were initially generated, the lowest mode (mode-1) was dominant and was typically found to be the only significant mode after the maximum surface displacement fell below 1 cm. The frequency of the mode-1 wave depended upon whether the pivot was along the long edge of the tank (in which case $L = 18.05$ cm) or along the short edge of the tank (in which case $L = 23.75$ cm). Taking the wave number to be $k = \pi/L$, the combination kH was always greater than 3, and so the waves were well approximated by deep water waves with frequency expected to be $\omega = \sqrt{gk}$. This prediction was born out through analysis of the experiments.

Each experiment was recorded with a digital camera placed 0.5 m from the face of the tank having the lens level with or slightly above the height of the surface. Movies were recorded at a rate of 30 frames per second (fps). Snapshots taken from a typical experiment are shown in Fig. 3. Here the six snapshots span approximately one period of the mode-1 wave. In this experiment the camera lens lies moderately above the height of the interface showing that the wave motion is effectively two-dimensional with negligible variations along the span of the tank. While most of the particles are clear, the displacement of eight dyed particles from one time to the next can be seen.

While the particles move up and down with the wave, as expected, it is clear that the horizontal distance between the particles change. It is this relative motion between particles that alternately draw interstitial fluid between them as they separate and push the fluid out as they reapproach that we propose is the main mechanism for damping and finite-time arrest of surface waves by particles.

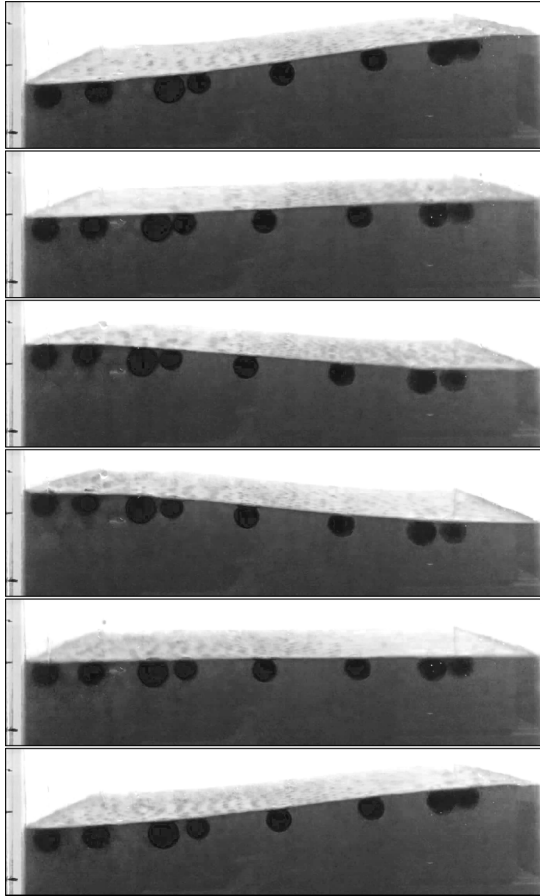


FIG. 3. Snapshots from an experiment with $L = 23.75$ cm, $D = 2.1$ cm and $d_p = 0.8$ cm. Some larger diameter dark-dyed particles are situated near the front wall of the tank to help visualize the relative particle motion. From top to bottom snapshots are successively taken every 0.10 s beginning 9.10 s after the tank is brought to its untilted position.

B. Analysis methods

From any snapshot the surface elevation at the front side of the tank can be determined from the left to right of the tank using the image processing software in MATLAB. Performing this analysis at successive times, a time series of surface elevation is constructed as shown in Fig. 4(a). Such images clearly show the dominant motion is that of a mode-1 wave with crests and troughs alternately peaking on the left and right sides of the tank. The amplitude $A(t)$ of the mode-1 wave is found by finding a best-fit cosine of the form $A \cos(\pi x/L)$ to the surface displacement at successive times. Here $x = 0$ and $x = L$ correspond, respectively, to the left and right sides of the tank. The result is shown in Fig. 4(b).

The focus of our analysis is upon the time dependence of the decaying wave amplitude. The amplitude envelope $\mathcal{A}(t)$ is constructed from $A(t)$, which is sampled at the discrete frame rate of 30 fps. First the time and magnitude of the amplitude at each (positive or negative) peak is determined through quadratic interpolation of three successive points of $A(t)$ about each peak. The values of \mathcal{A} are given by the average of successive pairs of peak values and the time of each value is given by the average of the times of each peak. The period is given by the difference between these times.

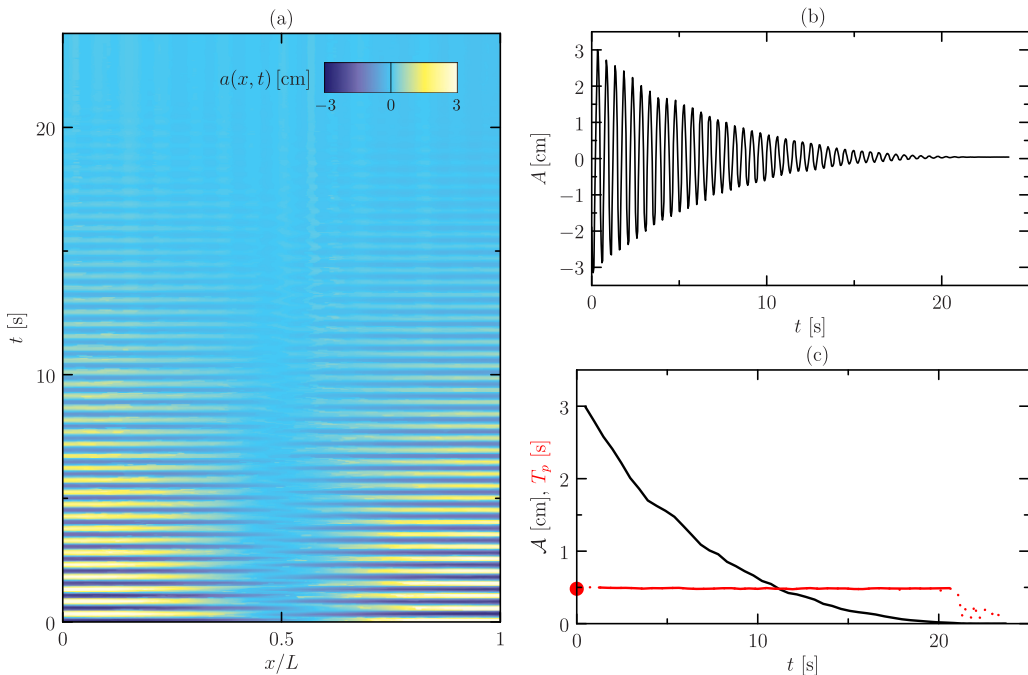


FIG. 4. (a) Time series of surface displacement, (b) mode-1 amplitude as it changes in time, and (c) the amplitude envelope (black) and period (red). In the last plot the dotted red line shows the period recorded at every point whereas the solid red line shows the filtered period versus time, keeping only those points within 1% of the theoretical value. The predicted period is indicated by the red circle at $t = 0$. These results are shown for an experiment with $L = 18.05$ cm, $D = 2.0$ cm, and $d_p = 1.1$ cm.

The results of this analysis applied to the values of $A(t)$ plotted in Fig. 4(b) is shown in Fig. 4(c). The monotonically decreasing curve is not entirely smooth. Fluctuations at early times are attributed primarily to the presence of higher mode number disturbances and to the moderately large-amplitude motion of the mode-1 wave whose steepness, $\mathcal{A}k = \mathcal{A}\pi/L$, when $\mathcal{A} = 1$ cm is 0.13 for $L = 23.75$ cm and 0.17 for $L = 18.05$ cm. At later times the fluctuations are attributed to values of $\mathcal{A}(t)$ being less than approximately 0.05 cm, close to the vertical pixel resolution of digital movies recording the amplitude. Correspondingly, we find that the measured period is nearly constant until the amplitude becomes too small. In examining the time dependence of \mathcal{A} at late times, only those values of \mathcal{A} having a corresponding period within 1% of the predicted theoretical value $2\pi(gk)^{-1/2}$ are used in the analysis.

For experiments with no particles, we find that the amplitude envelope decays exponentially up to the time when the amplitude is so small that it can no longer be detected. For example, Fig. 5(a) plots the amplitude envelope versus time in an experiment with no particles ($H = 23.0$ cm, $L = 23.75$ cm) and Fig. 5(b) replots \mathcal{A} on a log axis. The decay is not exponential at early times when the wave steepness is relatively large ($\mathcal{A}k \gtrsim 0.05$). However, the decay is well represented by an exponential after the amplitude becomes small. The e-folding decay time is $\tau = 9.58(\pm 0.08)$ s, in comparison to the order-of-magnitude estimate of $\tau_0 \simeq 14.2$ s from (1).

With particles floating on the surface, we find that the amplitude envelope decays approximately exponentially at early times. Figure 5 replots \mathcal{A} shown in Fig. 4(c) using log-linear axes. Consistent with exponential decay, the logarithm of \mathcal{A} decreases linearly at early times when the wave steepness is larger than ~ 0.05 . A best-fit line through the curve for \mathcal{A} lying in the range between 1.5 and 0.5 cm gives an e-folding decay time of $\tau = 5.43(\pm 0.08)$ s. Comparing this to the results of the

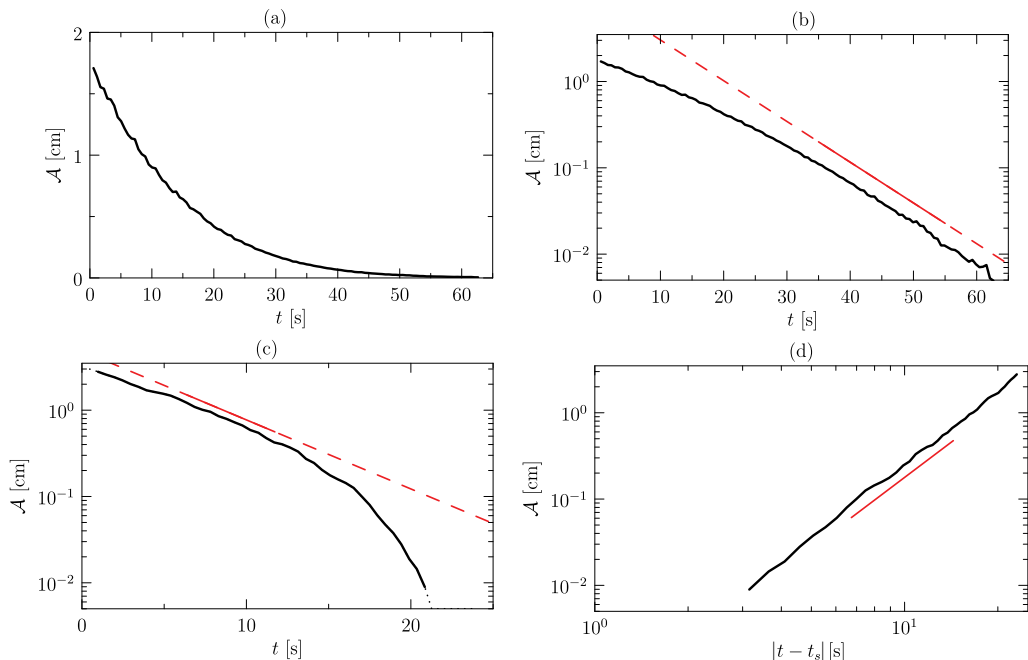


FIG. 5. Amplitude envelope \mathcal{A} as it evolves in time for an experiment (a) with no particles. These data are also presented in a log-plot in (b) with an offset best-fit line for $0.02 \text{ cm} < \mathcal{A} < 0.2 \text{ cm}$. Also, from the experiment with $d_p = 1.1 \text{ cm}$ diameter particles to depth $D = 2.0 \text{ cm}$ for which amplitude envelope vs time is plotted in Fig. 4(c), the data are reproduced as (c) a log-plot for all data (dotted line) and filtered data (thick black line), with offset best-fit line for $0.5 \text{ cm} < \mathcal{A} < 1 \text{ cm}$. The data in (c) are replotted in (d) as a log-log plot of amplitude vs time before stopping time $t_s = 24 \text{ s}$ for filtered data (thick black line), with offset best-fit line for $0.05 \text{ cm} < \mathcal{A} < 0.5 \text{ cm}$. In (b)–(d), the offset best-fit line is plotted as solid red over the fit range and, in (b) and (c), is extrapolated as a dashed line.

experiment with no particles, it is apparent that particles enhance linear damping and act effectively even for waves with large steepness.

After the period of exponential decay, the amplitude falls more sharply, exhibiting a power law dependence of the form $(t_s - t)^q$. We determine the stopping time t_s and power law exponent q from a best-fit through values of the amplitude envelope for $0.05 \text{ cm} < \mathcal{A} < 0.5 \text{ cm}$. This is plotted in Fig. 5(d). In this case $t_s = 24(\pm 4) \text{ s}$ and $q = 2.67(\pm 0.05)$. Although the error in q is small for $t_s = 24 \text{ s}$, it varies by approximately 0.5 as t_s varies by its standard deviation.

C. Experiment results

The analyses described above are applied to the results of several experiments, most of which involved hydrogel beads as the floating particles. We first consider the exponential damping times measured for waves in a tank with no floating particles. These are indicated by the solid circles in Fig. 6. As mentioned above, although τ_0 given by (1) is an order-of-magnitude estimate of the damping time, it overpredicts the actual damping time by a factor of about two-thirds.

When particles are present, the e-folding time for decay of the wave at early times decreases significantly, being set by the depth of the particle layer, but not by the diameter of the particles. A best-fit power law through the data in Fig. 6 with $kD > 0.3$ suggests that

$$\tau \simeq (0.125 \pm 0.015)(kD)^{-1.05 \pm 0.20} \tau_0. \quad (9)$$

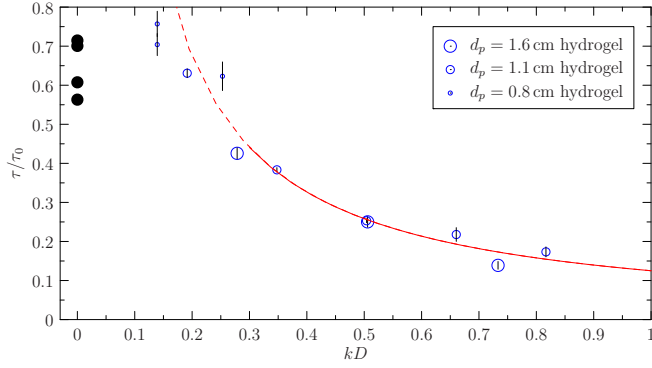


FIG. 6. Relative exponential damping time at early times versus particle depth times wave number. Solid circles correspond to experiments with no particles. Open circles correspond to experiments with floating spherical hydrogel beads having particle diameter as indicated in the legend. The vertical lines indicate the associated errors. The solid red line indicates the best-fit power law with the dashed line extrapolating to lower values of kD .

In terms of the thin-film timescale τ_k , the exponential damping time when the wave steepness is larger than 0.05 is $\tau \simeq (0.112 \pm 0.014)(kD)^{-1.05 \pm 0.20} \tau_k$.

The characteristics of the late-time amplitude decay are shown in Fig. 7. The stopping time t_s is measured as the time for wave motion to be undetectable after the time when the amplitude of the

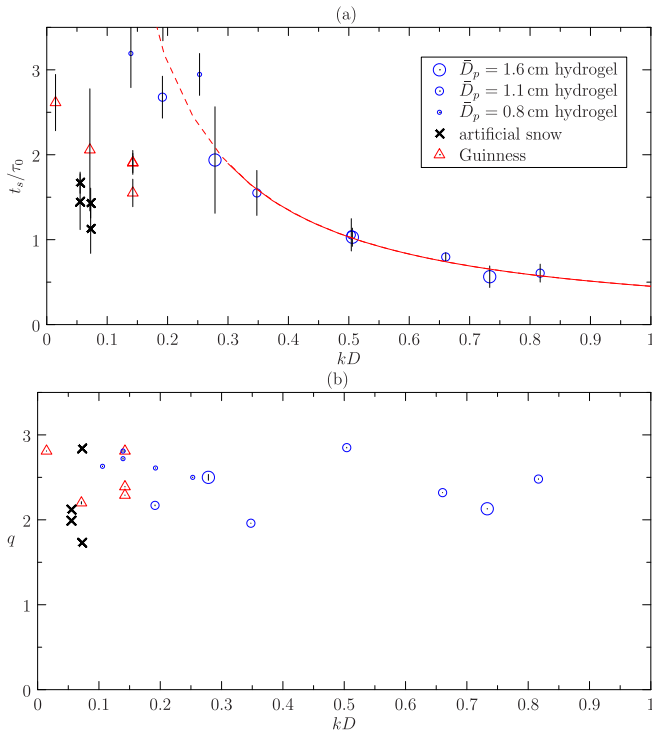


FIG. 7. (a) Relative stopping time and (b) power law exponent versus relative particle layer depth measured for experiments in which floating particles (circles), foam (triangles), and artificial snow (crosses) were present. Vertical lines indicate measured errors.

waves was measured to be 1 cm, corresponding to a wave steepness of 0.13 (0.17) if $L = 23.75$ cm (18.05 cm). This is plotted relative to τ_0 , and illustrates how the waves arrest their motion in a time less than τ_0 if the particle depth is sufficiently large relative to the inverse wave number of the waves. The best-fit power law to the points with $kD > 0.3$ is given by

$$t_s \simeq (0.45 \pm 0.03)(kD)^{-1.19 \pm 0.13} \tau_0, \quad (10)$$

or, in terms of τ_k , $t_s \simeq (0.40 \pm 0.03)(kD)^{-1.19 \pm 0.13} \tau_k$.

Figure 7(b) plots the corresponding power law exponents q . Although the measurements of q depend sensitively on the value of t_s , it is clear that the amplitude falls to zero as $(t_s - t)^q$ with q lying in the range between 2 and 3, independent of the particle layer depth.

In addition to results for experiments with spherical hydrogel beads, Fig. 7 also shows the stopping time and power law measured in experiments in which a layer of either foam from Guinness beer or artificial snow covered the surface. In the later case, the temperature of the water in the tank was cooled to nearly 0° C and the artificial snow was frozen so as to inhibit the rapid absorption of salt water into the fine sodium polyacrylate particles. Both sets of experiments show that the relative stopping time occurs sooner compared to experiments with hydrogel beads having comparable layer depth. However, the power law exponent of the time to stopping again lies in a range between 2 and 3. Although it lies beyond the scope of this paper to perform a detailed examination of damping by foam and artificial snow, the results serve to demonstrate that finite time arrest occurs when the surface is covered with a layer of fluids with more complex rheology although the relative importance of side wall [20,21] versus interior damping remains unclear.

IV. SCALING ANALYSIS

Sloshing modes in a rectangular tank experience enhanced dissipation when the fluid surface is impregnated with layers of floating particles. The elevated dissipation acts as a traditional linear damping at early times and higher seiche amplitudes; the form of this dissipation changes at later times and lower amplitudes, where it brings motion to rest in finite time. We conjecture that the straining and shearing of the particle layer by the sloshing mode periodically draws in and expels fluid from between the particles to provide the enhanced dissipation. Moreover, at large amplitudes, the particle lattice is broken apart to create an essentially linear damping mechanism; but as the seiche subsides, the particles approach one another and lock back up into a jammed lattice to provide an effective nonlinear damping. Analysis of our experimental results suggests that the early (exponential) damping time and the eventual stopping time are both inversely proportional to the depth of the particle layer. The final evolution of the sloshing amplitude \mathcal{A} is consistent with a power law decay with an exponent between 2 and 3. This suggests an energy dissipation mechanism that depends on a power of the seiche amplitude as \mathcal{A}^p , with p ranging between 3/2 and 5/3.

For a single-phase medium with a nonlinear viscosity $\mu(\dot{\gamma})$ that depends on the shear rate $\dot{\gamma}$, the observed decay exponent implies a shear-thinning power law rheology of the form $\mu = K\dot{\gamma}^{n-1}$ with $1/2 < n < 2/3$ [the corresponding dissipation rate being $\langle \mu(\dot{\gamma})\dot{\gamma}^2 \rangle \sim \mathcal{A}^{n+1}$]. Although this nonlinear rheology does not correspond to a plastic medium that genuinely jams at a yield stress of τ_Y (for which the dissipation rate would be $\tau_Y \dot{\gamma} \sim \mathcal{A}$), such shear-thinning behavior is common for suspensions. Nevertheless, the floating, periodically consolidating pack of relatively large hydrogel particles is likely poorly modelled as a single-phase complex fluid.

Instead we use scaling analysis to consider three simple scenarios that lead to enhanced dissipation beyond that of the fluid moving against the side walls of the tank. The first two predict exponential damping, while the last gives a plausible explanation for power law decay, even though the power law exponent differs from observations, for reasons conjectured thereafter.

In the first scenario, consider an idealized circumstance in which a sinusoidally displaced mode-1 surface wave draws particles up and down the sides of the tank and displaces them from one another within the bulk, as illustrated in Fig. 1. The dissipation occurring against the sides is straightforward to estimate: when the surface is displaced sinusoidally with a small amplitude $A = \mathcal{A} \sin \omega t$, the

shear arising adjacent to the sidewall is of order $\omega A/\Delta$ where $\Delta(t)$ is the (time-dependent) thickness of the fluid layer buffering the particles from the walls. Given that the particles are spherical with radius R , the effective contact area between the particles and wall is $O(\Delta R)$. Thus, the dissipation rate expected over this layer is expected to be of order

$$\varepsilon_l \sim \mu \frac{D}{R} \frac{L+W}{R} \left\langle \frac{\omega^2 \mathcal{A}^2}{\Delta^2} \Delta^2 R \right\rangle \sim \mu (\omega \mathcal{A})^2 \frac{D}{R} (L+W), \quad (11)$$

where the angular brackets denotes a time average over the wave period, μ is the fluid molecular viscosity, D is the depth of the particle layer, L is the length of the tank in the direction of the seiche, and W is the width perpendicular to that direction. Being proportional to \mathcal{A}^2 , this rate translates to a linear damping proportional to the depth of the particle layer.

In the second scenario, we estimate the dissipation over the bulk of the particle layer due to particles consolidating and pulling apart like an accordion as the wave moves up and down. We suppose the particles touch each other in a consolidated pack when the surface is undisturbed. If the surface is then displaced with amplitude $A = \mathcal{A} \sin \omega t$, the length of the surface, displaced according to $a(x, t) = A \cos(kx)$, increases approximately to $L[1 + (Ak)^2/4]$. Thus the mean spacing between the particles is expected to be

$$\delta \sim \frac{1}{2} (Ak)^2 R = \frac{1}{2} (\mathcal{A}k)^2 R \sin^2(\omega t). \quad (12)$$

Given that the effective contact area is now δR , mass conservation demands that the separation or approach of the particles with a speed $\dot{\delta}$ generates a radial outflow from the contact area in a plane perpendicular to the line between between any particle pair. This is of order

$$\mathcal{W}_p \sim \frac{\dot{\delta} \sqrt{R\delta}}{\delta} \sim 2(\mathcal{A}k) R \omega \cot \omega t. \quad (13)$$

Note that the singularities in \mathcal{W}_p arise when $\delta \rightarrow 0$ and are not real: the minimum separation is limited by the divergence of lubrication pressure as $\delta \rightarrow 0$, which instead holds the particles apart and prevents genuine contact. The speed estimate in Eq. (13) suggests a total dissipation rate, occurring over all the gaps between the particles (each of which has volume $\delta^2 R$), of order

$$\varepsilon_p \sim \mu \frac{D}{R} \frac{L}{R} \frac{W}{R} \left\langle \frac{\mathcal{W}_p^2}{\delta^2} (\delta^2 R) \right\rangle \sim 4\mu (\omega \mathcal{A}k)^2 DLW. \quad (14)$$

In Eq. (14) we blithely ignored the divergence of \mathcal{W}_p for $\delta \rightarrow 0$. The estimate in Eq. (14) again implies a linear damping rate proportional to the particle layer depth.

In the third scenario we consider the driven percolation flow that results from the consolidating pack driving fluid downward through the particle pack even as the gap between the particles close or, conversely, drawing fluid through the small spaces between particles as the standing wave grows. When the seiche damps to low amplitude, the jamming of the particles back into a lattice constrains their motion more significantly. In particular, one expects that the lateral confinement of the particle layer by the walls of the tank prevents the particles from diverging sideways from one another. In this situation, the flux of fluid from the gaps between particles becomes collimated into vertical channels, as illustrated in Fig. 1(b). By volume conservation, the vertical flow below one layer of a pair of particles results from the horizontal divergence of the flow between them such that $(2R)\delta\mathcal{W}_p \simeq \pi R^2 \dot{\delta}$. This suggests a revision of the estimate in Eq. (13) to

$$\mathcal{W}_p \sim \frac{R\dot{\delta}}{\delta} \sim 2\omega R \cot \omega t. \quad (15)$$

Here \mathcal{W}_p now denotes the vertical flow that is either pressed from one layer of particles through the underlying particle layers as the pack consolidates or is drawn through the underlying particle layers as the pack laterally expands. Being amplitude independent, the associated dissipation rate

$$\varepsilon_p \sim 4\mu \omega^2 DLW \quad (16)$$

is likewise independent of amplitude. Thus the damping is expected to depart from an exponential form and the seiche should halt in finite time. In particular, this estimate suggests that $p = 0$ for the simple model of Sec. II, which in turn implies a power law decay of $q = \frac{1}{2}$. Evidently, this form of damping is too extreme in comparison to our experimental observations, suggesting that the flow in and out of the gaps between particles may not be collimated completely away from the horizontal direction to vertically inflate and compress the particle layer. The model also neglects the expulsion of particles from the base of the particle pack as a result of the strong percolating flows that occur during consolidation and it assumes a homogeneous expansion and contraction of the pack, neglecting the fact that some particles may clump together, so resisting the extreme pressures involved with flow through tight spaces between particles. Modelling such complex processes goes well beyond simple scaling theory.

In any event, the simple model of damping incurred by the squeeze flow of particles into and out of the thin gaps between particles illustrates how a layer of floating particles may control the damping of sloshing modes *via* both a linear and nonlinear mechanism. By contrast, the shear layers at the sides of the tank likely only enhances the linear damping rate (at least provided the contact line does not play an important role [21–23]).

V. DISCUSSION AND CONCLUSION

Experiments measuring the decay in amplitude of a surface wave having layers of particles floating beneath the surface clearly show early-time exponential damping followed by a finite-time arrest approaching zero amplitude as a power law with exponent between 2 and 3. Through scaling estimates of energy dissipation by flows in the viscous boundary layers against the side walls as they are influenced by particles, by flows between particles, and by flows forced through particles by expanding and contracting particle separations above, we argue that the last is primarily responsible for the finite-time arrest. A simple scaling argument based upon these dynamics predicts a finite-time arrest occurs as a power law with exponent $1/2$, which is lower than the observed power law. We attribute the discrepancy to the complicated dynamics neglected by our theory that assumes the separation between particles is uniform in space as the pack expands and contracts. In reality, some particles clump together with large gaps forming between neighboring clumps, and particles at the base of the layer can themselves be ejected from the pack due to the strong downward flows generated by the consolidating pack. Modelling such dynamics lies beyond the scope of this work.

Because the influence of lateral boundaries arguably plays an insignificant role in the final stages of decay of the surface waves, our results could conceivably be extended to predict the termination of waves propagating into the marginal ice zone in the high-latitude oceans, a process that is often assumed to involve exponential damping alone [7,10,19,26–28], although Squire [15] recently suggested some observations might be better explained by an empirically determined power law. The early-time temporal exponential damping rate τ is recast [29] in terms of the spatial decay of a wave propagating with horizontal group velocity c_g through $k_i = 1/(c_g \tau)$, whose inverse is the e-folding decay length. From the expression below (9), we take $\tau \sim (kD)^{-1} \tau_k$. Also using the dispersion relation for deep water waves to write $k = \omega^2/g$, the spatial decay rate is predicted to vary with frequency according to

$$k_i \sim \omega^{11/2} D \nu^{1/2} g^{-3}. \quad (17)$$

Qualitatively, this correctly predicts the observed enhanced damping of high frequency waves. However, the exponent $11/2$ is larger than the frequency dependence with exponents between 2 and 4, which is typically observed for wave damping in the marginal ice zone [10]. Of course, the discrepancy could be attributed to limitations of the laboratory experiment in modeling realistic wave-ice interactions. However, it could also be an indication that damping becomes further enhanced when the wave amplitude is smaller than the depth of the ice layer thickness, in which case nonlinear damping by flow through the particle layer dominates the exponential damping timescale $\tau \sim \tau_p$. To put these conjectures on firmer footing, experiments are being planned on a larger scale

using floating particles more representative of frazil and pancake ice occurring in the marginal ice zone.

ACKNOWLEDGMENT

This research was performed, in part, through funding for both authors from the Natural Sciences and Engineering Research Council (NSERC) of Canada and the Woods Hole Oceanographic Institution GFD summer school program.

- [1] J. Thomson and W. E. Rogers, Swell and sea in the emerging Arctic Ocean, *Geophys. Res. Lett.* **41**, 3136 (2014).
- [2] A. L. Kohout, M. J. M. Williams, S. M. Dean, and M. H. Meylan, Storm-induced sea-ice breakup and the implications for ice extent, *Nature* **509**, 604 (2014).
- [3] C. O. Collins, W. E. Rogers, A. Marchenko, and A. V. Babanin, *In situ* measurements of an energetic wave event in the Arctic marginal ice zone, *Geophys. Res. Lett.* **42**, 1863 (2015).
- [4] F. Montiel and V. A. Squire, Modelling wave-induced sea ice break-up in the marginal ice zone, *Proc. R. Soc. A* **473**, 20170258 (2017).
- [5] V. A. Squire, Past, present, and impending hydroelastic challenges in the polar and subpolar seas, *Phil. Trans. R. Soc. A* **369**, 2813 (2011).
- [6] M. J. Doble, G. De Carolis, M. H. Meylan, J.-R. Bidlot, and P. Wadhams, Relating wave attenuation to pancake ice thickness, using field measurements and model results, *Geophys. Res. Lett.* **42**, 4473 (2015).
- [7] F. Montiel, V. A. Squire, and L. G. Bennetts, Attenuation and directional spreading of ocean wave spectra in the marginal ice zone, *J. Fluid Mech.* **790**, 492 (2016).
- [8] V. A. Squire and F. Montiel, Evolution of directional wave spectra in the marginal ice zone: A new model tested with legacy data, *J. Phys. Oceanogr.* **46**, 3121 (2016).
- [9] P. Sutherland and J.-C. Gascard, Airborne remote sensing of ocean wave directional wavenumber spectra in the marginal ice zone, *Geophys. Res. Lett.* **43**, 5151 (2016).
- [10] M. H. Meylan, L. G. Bennetts, J. E. M. Mosig, W. E. Rogers, M. J. Doble, and M. A. Peter, Dispersion relations, power laws, and energy loss for waves in the marginal ice zone, *J. Geophys. Res.* **123**, 3322 (2018).
- [11] J. B. Keller, Gravity waves on ice-covered water, *J. Geophys. Res.* **103**, 7663 (1994).
- [12] N. J. Balmforth and R. V. Craster, Ocean waves and ice sheets, *J. Fluid Mech.* **395**, 89 (1999).
- [13] R. Wang and H. H. Shen, Gravity waves propagating into an ice-covered ocean: A viscoelastic model, *J. Geophys. Res.* **115**, C06024 (2010).
- [14] J. E. M. Mosig, F. Montiel, and V. A. Squire, Comparison of viscoelastic-type models for ocean wave attenuation in ice-covered seas, *J. Geophys. Res.* **120**, 6072 (2015).
- [15] V. A. Squire, A fresh look at how ocean waves and sea ice interact, *Phil. Trans. R. Soc. A* **376**, 20170342 (2018).
- [16] S. Martin and P. Kauffman, A field and laboratory study of wave damping by grease ice, *J. Glaciol.* **27**, 283 (1981).
- [17] K. Newyear and S. Martin, A comparison of theory and laboratory measurements of wave propagation and attenuation in grease ice, *J. Geophys. Res.* **102**, 25091 (1997).
- [18] R. Wang and H. H. Shen, Experimental study on surface wave propagating through grease-pancake ice mixture, *Cold Regions Sci. Tech.* **61**, 90 (2010).
- [19] A. Toffoli, L. G. Bennetts, M. H. Meylan, C. Cavaliere, A. Alberello, J. Elsnaab, and J. P. Monty, Sea ice floes dissipate the energy of steep ocean waves, *Geophys. Res. Lett.* **42**, 8547 (2015).
- [20] A. Sauret, F. Boulogne, J. Cappello, E. Dressaire, and H. A. Stone, Damping of liquid sloshing by foams, *Phys. Fluids* **27**, 022103 (2015).

- [21] F. Viola, P.-T. Brun, B. Dollet, and F. Gallaire, Foam on troubled water: Capillary induced finite-time arrest of sloshing waves, [Phys. Fluids](#) **28**, 091701 (2016).
- [22] F. Viola, P.-T. Brun, and F. Gallaire, Capillary hysteresis in sloshing dynamics: A weakly nonlinear analysis, [J. Fluid Mech.](#) **837**, 788 (2018).
- [23] F. Viola and F. Gallaire, A theoretical framework to analyze the combined effect of surface tension and viscosity on the damping rate of sloshing waves, [Phys. Rev. Fluids](#) **3**, 094801 (2018).
- [24] J. E. Weber, Wave attenuation and wave drift in the Marginal Ice Zone, [J. Phys. Oceanogr.](#) **17**, 2351 (1987).
- [25] G. Sutherland, T. Halsne, J. Rabault, and A. Jensen, The attenuation of monochromatic surface waves due to the presence of an inextensible cover, [Wave Motion](#) **68**, 88 (2017).
- [26] P. Wadhams, Attenuation of swell by sea ice, [J. Geophys. Res.](#) **78**, 3552 (1973).
- [27] V. A. Squire, J. P. Dugan, P. Wadhams, P. J. Rottier, and A. K. Liu, Of ocean waves and sea ice, [Annu. Rev. Fluid Mech.](#) **27**, 115 (1995).
- [28] F. Arduin, P. Sutherland, M. Doble, and P. Wadhams, Ocean waves across the Arctic: Attenuation due to dissipation dominates over scattering for periods longer than 19s, [Geophys. Res. Lett.](#) **43**, 5775 (2016).
- [29] M. Gaster, A note on the relation between temporally-increasing and spatially-increasing disturbances in hydrodynamic stability, [J. Fluid Mech.](#) **14**, 222 (1962).